



ELSEVIER

Earth and Planetary Science Letters 205 (2003) 361–378

EPSL

www.elsevier.com/locate/epsl

Plume capture by divergent plate motions: implications for the distribution of hotspots, geochemistry of mid-ocean ridge basalts, and estimates of the heat flux at the core–mantle boundary

A. Mark Jellinek*, Helge M. Gonnermann, Mark A. Richards

Department of Earth and Planetary Science, University of California, Berkeley, CA 94720, USA

Received 21 June 2002; received in revised form 14 October 2002; accepted 30 October 2002

Abstract

The coexistence of stationary mantle plumes with plate-scale flow is problematic in geodynamics. We present results from laboratory experiments aimed at understanding the effects of an imposed large-scale circulation on thermal convection at high Rayleigh number ($10^6 \leq Ra \leq 10^9$) in a fluid with a temperature-dependent viscosity. In a large tank, a layer of corn syrup is heated from below while being stirred by large-scale flow due to the opposing motions of a pair of conveyor belts immersed in the syrup at the top of the tank. Three regimes are observed, depending on the ratio V of the imposed horizontal flow velocity to the rise velocity of plumes ascending from the hot boundary, and on the ratio λ of the viscosity of the interior fluid to the viscosity of the hottest fluid in contact with the bottom boundary. When $V \ll 1$ and $\lambda \geq 1$, large-scale circulation has a negligible effect on convection and the heat flux is due to the formation and rise of randomly spaced plumes. When $V > 10$ and $\lambda > 100$, plume formation is suppressed entirely, and the heat flux is carried by a sheet-like upwelling located in the center of the tank. At intermediate V , and depending on λ , established plume conduits are advected along the bottom boundary and ascending plumes are focused towards the central upwelling. Heat transfer across the layer occurs through a combination of ascending plumes and large-scale flow. Scaling analyses show that the bottom boundary layer thickness and, in turn, the basal heat flux q depend on the Peclet number, Pe , and λ . When $\lambda > 10$, $q \propto Pe^{1/2}$ and when $\lambda \rightarrow 1$, $q \propto (Pe\lambda)^{1/3}$, consistent with classical scalings. When applied to the Earth, our results suggest that plate-driven mantle flow focuses ascending plumes towards upwellings in the central Pacific and Africa as well as into mid-ocean ridges. Furthermore, plumes may be captured by strong upwelling flow beneath fast-spreading ridges. This behavior may explain why hotspots are more abundant near slow-spreading ridges than fast-spreading ridges and may also explain some observed variations of mid-ocean ridge basalt (MORB) geochemistry with spreading rate. Moreover, our results suggest that a potentially significant fraction of the core heat flux is due to plumes that are drawn into upwelling flows beneath ridges and not observed as hotspots.

© 2002 Elsevier Science B.V. All rights reserved.

* Corresponding author. Tel.: +1-510-642-6331; Fax: +1-510-643-9980.

E-mail address: markj@seismo.berkeley.edu (A.M. Jellinek).

Keywords: mantle convection; mantle plume; plume–ridge interaction; mid-ocean ridge basalt geochemistry; core heat flux

1. Introduction

Mantle plumes ascending from the core–mantle boundary probably cause volcanic hotspots [1,2]. However, the coexistence of narrow, relatively stationary plumes and plate-scale convection has yet to be demonstrated in either laboratory or numerical models (e.g. [3]). Geophysical and geochemical observations show the effects of mantle plumes on nearby mid-ocean ridges [4–10], and a number of modeling studies have addressed plume–ridge interactions (e.g. [10–23]). However, with the exception of parameterized numerical investigations of the interaction between mantle stirring and ascending plumes by Steinberger and O’Connell [24,25] and Steinberger [26], most numerical and laboratory studies have focused on the interactions between plumes in the upper mantle with the lithosphere. Moreover, no work to date has investigated the importance of plate-driven mantle circulation on the formation and rise of plumes from a thermal boundary layer at the base of the mantle.

In this study we examine the influence of plate-driven flow on the formation and distribution of plumes and on the heat flux at the core–mantle boundary. Using laboratory experiments we first map the nature of the interaction between an imposed large-scale flow and plumes rising from a hot boundary layer across a wide range of dynamical conditions appropriate to the Earth’s mantle. This aspect of our work extends the results of an earlier study performed by Kincaid et al. [23], which addressed the interaction between mid-ocean ridges and convection in the upper mantle. Furthermore, we expand the analysis of Kincaid et al. to include the additional important influence of viscosity variations in the hot thermal boundary layer. Next, we compare measurements of the (local) basal heat flux with scaling theories developed to understand the influence of large-scale flow and viscosity variations on the formation of plumes and, in turn, the heat transfer in a basally heated mantle. Our heat flux analysis and experimental results are then used to discuss

the reliability of current estimates of the core heat flux based on studies of hotspots. Next, we apply our results in developing new interpretations of the global distribution of hotspots and the variation of MORB chemistry with spreading rate. We conclude with a brief discussion of outstanding questions and directions for future work.

2. Experiments

2.1. Experimental setup, conditions and methods

Our convection experiments are conducted in a large (1.5 m × 1.5 m by 0.6 m deep) tank that is filled with corn syrup, which has a viscosity that decreases strongly with increasing temperature (Fig. 1, Table 1). The sidewalls are glass-insulated with 20 cm of Styrofoam insulation; an aluminum heat exchanger through which hot water is circulated forms the base of the tank. The heat exchanger is designed such that the maximum horizontal temperature variation across the hot boundary (from the inlet to the outlet) is less than about 1°C during an experiment. Furthermore, the aluminum plate forming the top of the heat exchanger is sufficiently thin that thermal fluctuations due to convection in the overlying syrup are damped quickly relative to the time scale for convective instability and the formation of plumes. Hence, we achieve an isothermal lower boundary condition. Immersed in the syrup at the top of the tank are two conveyor belts, the opposing motions of which are used to generate a large-scale flow that is divergent at the center of the tank and convergent at opposite sidewalls. Our experiments are characterized quantitatively using time series of measurements of basal flux and temperature along with shadowgraphs, time-lapse video and still images (Fig. 1). Direct measurements of the local basal heat flux are made using Omega HFS-4 thermopile sensors. An array of thermocouples is used to obtain temperature measurements at the floor and sidewalls of the tank as well as vertical temperature profiles in the fluid

interior. All invasive sensors are located below conveyor belt 1 so that the (symmetrical) flow beneath conveyor belt 2 is unperturbed by sensors. In each experiment, comparison of shadowgraphs of the motions beneath both conveyor belts indicates that the sensors have no significant influence on the flow.

Measured temperature gradients across the sidewalls of the tank are used to quantify the heat loss to these boundaries, which is, in turn, applied to better understand the dynamical influence of the boundary conditions of the tank on the flow. Although the sidewalls are well insulated, cooling to the air in the laboratory, which is maintained at a constant temperature $T_1 = 20^\circ\text{C}$, is unavoidable and produces a very weak buoy-

ancy flux that drives downwellings along the tank walls and, thus, large-scale circulation in the tank. However, we find that the resulting large-scale flow significantly influences the thickness and dynamics of the thermal boundary layer only when the velocities of the downwellings along the sidewalls are comparable to the characteristic rise velocity of upwelling plumes V_p , and to the imposed belt velocity, V_b , when $V_b \ll V_p$. Because of the inherent complexity of a large-scale flow driven by cooling to four boundaries we restrict our analysis of the basal heat flux in the presence of imposed large-scale circulation to the situation in which $V_b \geq V_p$ and where V_b is much greater than the downwelling velocities along the sidewalls.

The thermal boundary condition at the top of

Table 1
Parameters used in calculations

Parameter	Symbol	Value and/or unit
Average horizontal fluid velocity due to conveyor belts	U	m s^{-1}
Coefficient of thermal expansion of the corn syrup	α	$5.61 \times 10^{-4} \text{ } ^\circ\text{C}^{-1}$
Conveyor belt velocity	u_{belt}	m s^{-1}
Density of syrup ^a	ρ	kg m^{-3}
Dynamic viscosity of syrup ^b	μ	Pa s
Gravitational acceleration	g	9.8 m s^{-2}
Heat flux	q	W m^{-2}
Height of thermal boundary layer	δ_t	m
Height of velocity boundary layer	δ_v	m
Horizontal flow velocity in the thermal boundary layer	u_t	m s^{-1}
Horizontal length scale	L	m
Plume rise velocity	V_p	m s^{-1}
Syrup layer depth	H	0.6 m
Tank width	w	1.5 m
Temperature difference across the hot boundary layer	ΔT	$^\circ\text{C}$
Thermal conductivity of the syrup ^c	K	$\text{W m}^{-1} \text{ } ^\circ\text{C}^{-1}$
Thermal diffusivity ^d	κ	$1 \times 10^{-7} \text{ m}^2 \text{ s}^{-1}$
Subscripts		
i	interior	
h	surface of hot boundary	
Superscripts		
f	free slip	
max	maximum	
n	no slip	
p	plume	

^a The density of ADM 62/44 corn syrup as a function of temperature $T^\circ\text{C}$ was measured by C. Jaupart (IPGP, Paris) and found to be $\rho(T) = 10^3(-5.60774 \times 10^{-4}T + 1.46201)$.

^b The viscosity of the ADM 62/44 corn syrup used in these experiments varied with temperature $T^\circ\text{C}$ according to $\mu(T) = 10^{-3} \exp(15.911279 - 0.18456T + 0.000778T^2)$ Pa s.

^c The thermal conductivity of the syrup as a function of temperature T was measured by C. Jaupart (IPGP, Paris) and found to be $K(T) = 0.365 + 0.00245T$.

^d The thermal diffusivity is approximately constant owing to a very weak temperature dependence of K .

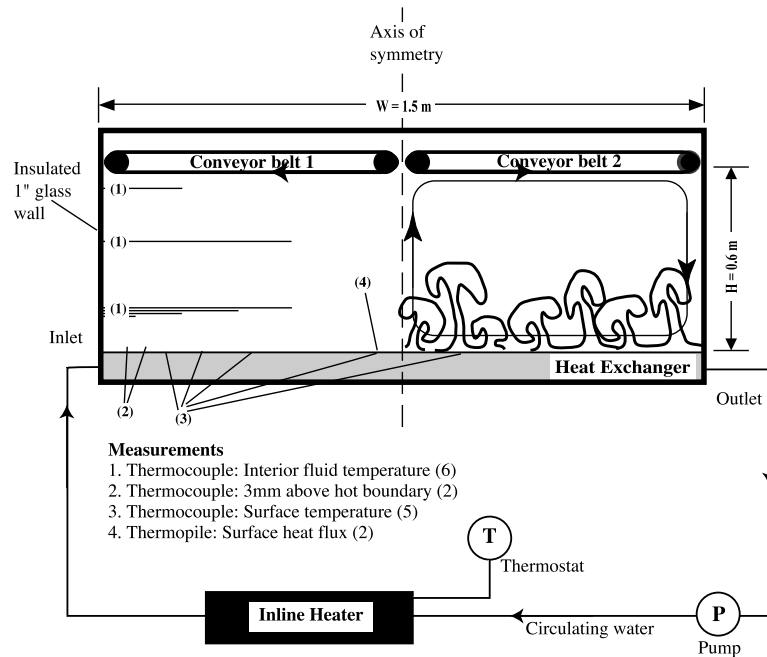


Fig. 1. A schematic drawing of the apparatus used in our convection experiments. See text for discussion.

the tank is complicated because the conveyor belts and, hence, also the syrup, are exposed to the air in the laboratory. Consequently, whereas the contribution of sidewall cooling to the flow is probably insignificant in all of our experiments in which $V_b \geq V_p$, the influence of surface cooling to the room on the flow varies with the belt velocity and the temperature of the syrup. However, the surface heat flux to the lab is always much smaller than the basal heat flux from the hot boundary, so that the tank heats up gradually during a typical experiment.

Prior to the start of our experiments the water in the heat exchanger, initially at room temperature, is pumped at a high rate through an ‘in-line heater’ set to a prescribed temperature using a thermostat. Initially, the rate of increase in water temperature, and, hence, the floor surface temperature is rapid, occurring on a time scale that is short compared to the time scale for plume formation. In response to this complicated and evolving boundary condition, the convection in the overlying syrup is highly time-dependent and spatially complex. Over time, however, the heat-

ing rate of the water declines and resultant transients to the hot boundary occur on time scales that are increasingly long compared with the time scale for plume formation. The floor surface temperature becomes constant over time scales that are long in comparison to the time scale for plume formation and quasi steady-state flow conditions are achieved [27].

2.2. Dimensionless parameters

In all of our experiments the Prandtl number $Pr = \mu_i / \rho \kappa$ is large ($> 10^4$), which enables us to investigate flows in which the influence of inertial forces is negligible (i.e. the Reynolds number Re , which is a ratio of inertial to viscous forces, is less than about 1). In addition, the aspect ratio of the fluid layer $A = w/H$ is constant and about 2.5. Here, μ_i is the fluid viscosity, ρ is the fluid density, κ is the average thermal diffusivity of the corn syrup, w is the width of the tank, and H is the depth of the fluid layer (Fig. 1, Table 1). The subscript ‘i’ refers to properties evaluated at the average interior fluid temperature. The nature of

the flow is characterized by two externally controlled parameters. The time dependence of convection from the hot boundary increases with the Rayleigh number:

$$\text{Ra} = \frac{\rho_i g \alpha \Delta T H^3}{\mu_i \kappa} \quad (1)$$

which may be viewed as the ratio of the time scale H^2/κ for thermal diffusion across the syrup layer to the time scale $\mu_i/\rho g \alpha \Delta T H$ required for a hot blob with diameter H to rise through the same distance. Here, g is the gravitational acceleration and α is the coefficient of thermal expansion and $\Delta T = (T_h - T_i)$ is the temperature difference from the hot boundary to the fluid interior. The subscript ‘h’ refers to properties evaluated at the surface of the hot boundary. Convective instability and plume formation occur at a critical Ra of order 10^3 .

The imposed large-scale flow velocity is represented non-dimensionally by the Peclet number:

$$\text{Pe} = \frac{UH}{\kappa} \quad (2)$$

which is the ratio of the time scale for thermal diffusion across the layer to the time scale H/U for the vertical advection of heat across the layer by flow due to the motion of the conveyor belts. Here, U is a scale for the imposed flow velocity due to the motion of the belts. Because horizontal (and vertical) velocities must vanish at the rigid hot boundary, velocities near the hot boundary, which influence the formation of plumes, are less than the imposed belt velocity, u_{belt} , which governs the ascent of plumes through the layer of corn syrup. In order to characterize motions near the hot boundary and in the fluid interior we thus take $U = u_{\text{belt}}/2$.

To characterize the influence of imposed large-scale stirring and viscosity variations on the dynamics of plume formation and rise through the full depth of the tank we introduce two internally defined parameters. The velocity ratio:

$$V = \frac{\text{Pe}}{c\text{Ra}^{1/3}} \quad (3)$$

is the ratio of the imposed horizontal velocity $U = \kappa\text{Pe}/H$ to the characteristic rise velocity of

plumes $V_p = c\kappa\text{Ra}^{1/3}/H$ [28,29]. The constant $c \approx 9$ is obtained from measurements of plume rise velocities obtained near the top of the thermal boundary layer. The inclusion of a constant in Eq. 3 is unusual because it is a characteristic velocity scale. However, as will be shown, defining V in terms of a measured rise velocity conveniently leads to a transition from a flow dominated by ascending plumes to a flow governed by large-scale flow when V is order 1. The viscosity ratio:

$$\lambda = \frac{\mu_i}{\mu_h} \quad (4)$$

is the ratio of the dynamic viscosity of the cold (interior) fluid above the thermal boundary layer to the dynamic viscosity of the (hot) fluid in contact with the hot boundary. It will be useful to note that the temperature at the hot boundary, and thus μ_h , is approximately constant over time scales much larger than the time scale for plume formation. Thus, from Eq. 1 $\lambda \propto 1/\text{Ra}$ and thus, as the tank warms during an experiment, Ra increases while λ decreases.

3. Qualitative effects of plate-driven flow on the formation, rise and distribution of plumes

Through a series of experiments we identify several flow regimes, depending on the velocity ratio V and the viscosity ratio λ (Fig. 2). For a given $\lambda \geq 1$, at small velocity ratios ($0 \leq V \leq 0.1$) the imposed large-scale circulation has a negligible influence on the convection. When $\lambda > 100$, hot low-viscosity fluid rises intermittently from the bottom boundary in plumes with large heads and narrow trailing conduits, as well as through persistent low-viscosity conduits left over from previous generations of plume-forming instabilities [27,30]. In this case, plumes ascend through the interior fluid and pond beneath the belts and generate no large-scale circulation, consistent with results from recent compositional convection experiments by Jellinek et al. [30] in which $V = 0$. We note that when $V > 0$, ponded plume material is ultimately stirred back into the fluid by the plate-driven flow. As V is increased to values of order 1 a transition occurs and the imposed flow

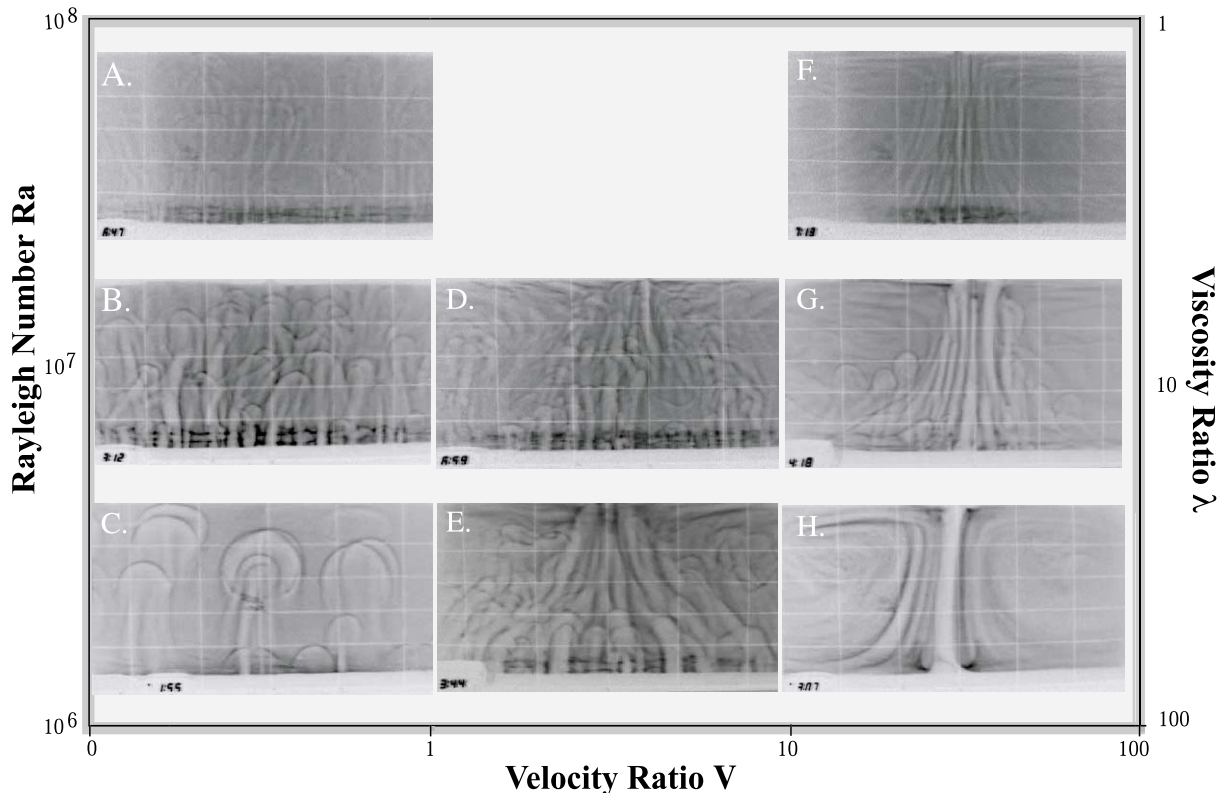


Fig. 2. A map of velocity ratio V –viscosity ratio λ –Rayleigh number Ra space summarizing the influence of imposed large-scale circulation on convection from a hot boundary across a broad range of conditions. Note the change in the style of flow that occurs when the velocity ratio $V \approx 1$. In all experiments shown, convection from the hot boundary is fully developed prior to turning on the belts. See text for discussion. Regimes: (A) $Ra = 4.0 \times 10^7$, $\lambda = 5.0$, $V = 0$; (B) $Ra = 9.5 \times 10^6$, $\lambda = 23$, $V = 0$; (C) $Ra = 2.0 \times 10^6$, $\lambda = 69$, $V = 0$; (D) $Ra = 3.0 \times 10^7$, $\lambda = 9.0$, $V = 5$; (E) $Ra = 3.5 \times 10^6$, $\lambda = 90$, $V = 8$; (F) $Ra = 5.0 \times 10^7$, $\lambda = 5$, $V = 37$; (G) $Ra = 3.8 \times 10^6$, $\lambda = 60$, $V > 10$; (H) $Ra = 2.5 \times 10^6$, $\lambda = 90$, $V = 20$.

causes thickening and thinning of the thermal boundary layer beneath the central upwelling and downwellings at the sidewalls, respectively. Plumes move along the lower boundary toward the central upwelling at a rate determined by the horizontal velocity at the top of the thermal boundary layer, while ascending plume heads and conduits are drawn towards the central upwelling at a rate governed by velocities in the fluid interior. At large velocity ratios ($V > 10$), and depending on λ , plume formation is increasingly suppressed over the distance between the sidewalls and the central upwelling. Plume suppression occurs either because the thermal boundary layer is insufficiently thick to form plumes, or because nascent plume instabilities are advected into the

central upwelling before they can grow into plumes. In the extreme case of $V > 10$ and $\lambda > 100$, the thermal boundary layer appears to be insufficiently thick to form plumes and all of the boundary layer fluid is advected horizontally into the central upwelling, where it forms a buoyant sheet. We note that the suppression of plume-driven flow is not simply due to a lower Ra [31,32] – the flow is plume-dominated in experiments conducted in the absence of imposed large-scale stirring.

The viscosity ratio λ has three effects on the flow. First, for a given temperature difference ΔT , the size and rise velocity of plume heads is determined by the boundary layer thickness, which depends on the viscosity of the interior flu-

id, μ_i . Second, the extent to which plumes interact with one another depends, in part, on the spacing between plume-forming instabilities [30], which is proportional to $\lambda^{1/3}$ [33,34]. Hence, with decreasing λ (or increasing Ra) plume heads have larger rise velocities and become both smaller and more closely spaced. The combination of these two effects leads to a more vigorous (i.e. time-dependent) overall flow but no large-scale circulation [30–32,35,36]. Third, the magnitude of λ determines the extent of vertical velocity gradients arising due to drag along the hot boundary, as well as the average horizontal fluid velocity in the thermal boundary layer. Whereas vertical velocity gradients determine the extent to which ascending plumes are drawn into the central upwelling, the horizontal fluid velocity in the thermal boundary layer apparently governs its thickness and influences the rate at which established conduits or, more generally, instabilities migrate downstream (Fig. 2).

Flow regimes comparable to those summarized in Fig. 2 are observed in an earlier study of the interaction between plumes ascending through the upper mantle and plate-driven flow performed by Kincaid et al. [23] (hereafter referred to as KSD). KSD report experiments conducted over a narrow range of Rayleigh numbers ($10^4 \leq \text{Ra} \leq 10^5$, where Ra is defined as by Eq. 1) and for dimensional spreading rates spanning those appropriate to the mid-Atlantic ridge and East Pacific Rise. The results of KSD can be compared with Fig. 2, considering constraints on V and λ . We note that the thermal diffusivity $\kappa = 10^{-6} \text{ m}^2 \text{ s}^{-1}$ used by KSD to calculate Ra is about a factor of 10 too large for the sucrose solutions used as working fluids. Correcting for this error (i.e. taking $\kappa = 10^{-7} \text{ m}^2 \text{ s}^{-1}$) implies the range $10^5 \leq \text{Ra} \leq 10^6$ for their experiments. The structure of the plumes (relative difference in the diameters of plume heads and conduits) observed in KSD's figure 9d,e, together with the small variation in Ra, suggest that λ is order 100 in most of their experiments. Therefore, the flows observed in these Ra– λ regimes are consistent with data shown in Fig. 2. Using Eq. 3 we recast the Ra-spreading rate data of KSD into V – λ space, where λ is taken to be 100. KSD results thus indicate that as-

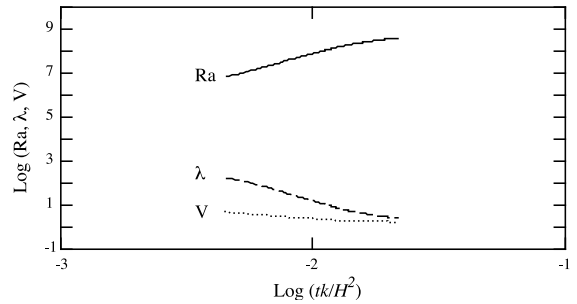


Fig. 3. Plot showing the time evolution of Ra, V and λ as the tank heats up during an experiment in which $\text{Pe} = 2 \times 10^4$.

ascending plumes are uninfluenced by large-scale flow when $V < 0.6$ and are drawn into a central sheet-like upwelling when $V > 5$. In intermediate regimes ($0.6 < V < 5$), plumes are focused towards the central upwelling, resulting in ‘strong axial variability’ (KSD, p. 16188). The results for $\text{Ra} \sim 10^6$ flows in Fig. 2 are therefore consistent with the findings of KSD.

The present study extends KSD in two ways. First, our experiments span two additional orders of magnitude in Ra space, thus mapping the flows over a wider range of conditions appropriate to the Earth's mantle. Second, Fig. 2 indicates that in addition to being governed by the velocity ratio V (or the total buoyancy flux as expressed through Ra), the flows depend on the viscosity ratio λ .

4. Influence of plate-driven flow on the mode of heat transfer from the hot boundary

Plume instabilities can form only if the thermal boundary layer has sufficient buoyancy to detach from the hot boundary. Therefore, for a given ΔT and μ_i , whether plumes form depends mostly on the thickness of the thermal boundary layer δ_t . Because mass must be conserved, horizontal (plate-driven) motions will cause the thermal boundary layer to thin upstream and thicken downstream. Furthermore, the basal heat flux, q , is proportional to $1/\delta_t$, and thus the downstream thickening of the thermal boundary layer implies a downstream reduction in q . In order to under-

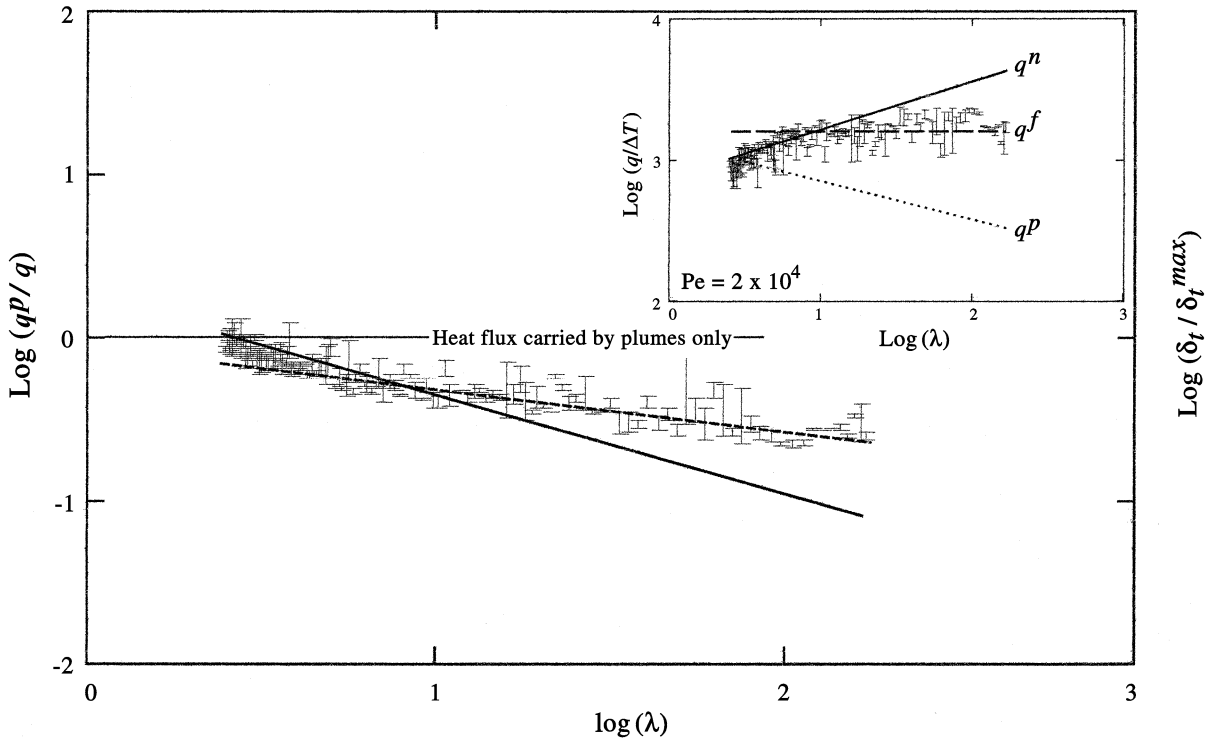


Fig. 4. Plots of the measured (local) basal heat flux ratio with uncertainties (crosses), q^p/q , and (inset) dimensional heat flux, q , as a function of the viscosity ratio, λ , using data from the experiment presented in Fig. 3. The inferred ratio of the actual thermal boundary layer thickness to the maximum thermal boundary layer thickness, δ_t/δ_t^{max} , corresponding to q^p/q is also indicated. The experiment evolves in time from right to left along the horizontal axes. As the tank heats up, Ra increases and λ decreases accordingly (see Fig. 3). When $q^p/q=1$, the thermal boundary layer is critically thick, $\delta_t = \delta_t^{max}$, and the heat flux is due to the formation and rise of plumes. When $q^p/q < 1$, $\delta_t < \delta_t^{max}$, and the heat flux is proportionally larger. Also shown are predictions for q^p/q and (inset) q based on the ‘free-slip’ theory (cf. Eq. 7, dashed line) and the ‘no-slip’ theory (cf. Eq. 10, solid line). q^p (dotted line) is indicated in the inset figure for reference. The predicted dimensional heat fluxes (inset only) have been normalized to ΔT , which declines monotonically by about a factor of 2 during this experiment, resulting in well-defined power laws. When λ is greater than about 5 (order 10) the average horizontal velocity in the thermal boundary layer is close to that imposed by the belts. In this case the mechanical boundary condition at the base of the tank is approximately ‘free-slip’ and the surface heat flux q is independent of λ and proportional to $Pe^{1/2}$. In contrast, when the viscosity ratio λ is less than about 5, drag along the hot boundary reduces the average horizontal flow velocity in the thermal boundary layer. The boundary condition is approximately ‘no-slip’ and q is proportional to $(Pe\lambda)^{1/3}$.

stand the quantitative influence of plate-driven circulation on δ_t and q we thus measure the *local* heat flux at two positions located a distance $0.45AH$ from the sidewall (Fig. 1) in an experiment in which the conveyor belt velocity is fixed and $Pe \approx 2 \times 10^4$. The combination of the imposed stirring and convection from the hot boundary during the experiment causes the tank to heat up, resulting in progressive reductions in λ and V , as well as an increase in Ra (although ΔT declines monotonically by about a factor of 2 as $T_i \rightarrow T_h$) (Fig. 3).

The maximum thickness to which a thermal boundary layer can grow corresponds to the thickness, δ_t^{max} , required to form plumes. Spatially averaged heat flux data from experiments in which $V=0$ indicate that the heat flux due to the formation and rise of plumes is approximately $q^p \approx 0.15(K\Delta T/H)Ra^{0.28}$, where K is the thermal conductivity of corn syrup, which implies $\delta_t^{max} \approx 6.67HRa^{-0.28}$. Thus, for convenience in interpretation, in Fig. 4 we plot the heat flux ratio q^p/q versus λ and obtain a measure of the importance of horizontal flow in the thermal boundary

layer to the local heat flux. When $q^p/q < 1$, large-scale flow leads to thinning of the thermal boundary layer and, thus, an increase in the heat flux over that which would occur by the formation and rise of plumes alone. It is useful to note that λ is chosen as the independent variable in Fig. 4 because under constant-Pe conditions, the magnitude of the viscous drag at the hot boundary, which is governed by λ , determines the average horizontal velocity in the thermal boundary layer [37,38]. In particular, V is not chosen for the x -axis because Pe is constant and whereas Ra governs δ_t^{\max} , buoyancy effects do not influence the vertical (diffusive) growth of a conductive thermal boundary layer.

In order to understand the data shown in Fig. 4 we present a scaling analysis for the thermal boundary layer thickness δ_t as a function of Pe and λ that is, in turn, applied to find scalings for the heat flux q . The conduction of heat from the bottom boundary causes a thermal boundary layer of hot, buoyant low-viscosity fluid to grow to a thickness δ_t , where $\delta_t \ll H$ (Figs. 2 and 5). Conservation of heat and mass in the thermal boundary layer requires that δ_t is determined by both the velocity, κ/δ_t , at which the boundary layer grows by thermal conduction and the average velocity u_t at which hot fluid within the thermal boundary layer is advected horizontally towards the central upwelling. The velocity u_t depends on the imposed velocity U and on the extent to which viscous drag along the rigid bottom boundary of the tank impedes horizontal fluid motion.

The importance of drag is indicated by the height to which vertical velocity gradients extend from the hot boundary and form a velocity boundary layer with thickness δ_v . Examination of the results summarized in Fig. 2 indicates that δ_v depends on the viscosity ratio λ . Due to an approximately exponential dependence of the viscosity of corn syrup on temperature, when $\lambda > 100$ vertical velocity gradients are observed to be confined to a narrow region comprising roughly the bottom 10–15% of the thermal boundary layer [37,38]. Hence, $\delta_v \ll \delta_t$ and the imposed overturning motions are essentially decoupled from the boundary. Consequently, most

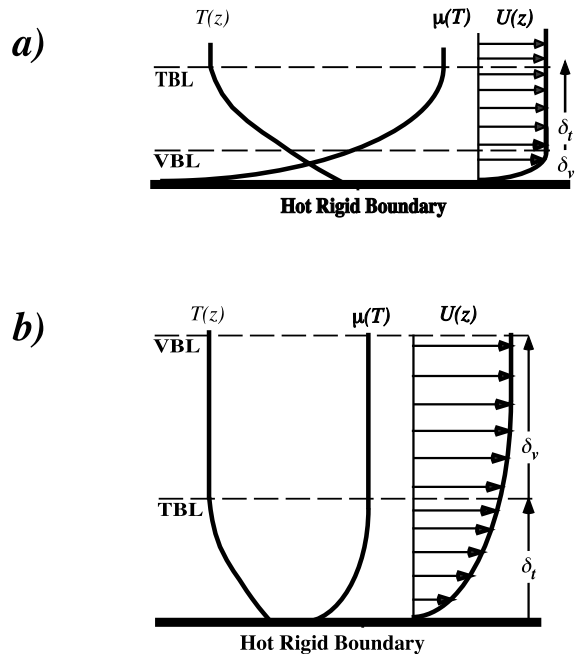


Fig. 5. Definition sketches illustrating the approximate structure of the flow above the hot boundary when (a) $\lambda > 10$ and (b) $\lambda \sim 1$. The conduction of heat from the hot boundary causes the growth of a thermal boundary layer (TBL). Viscous drag along the hot boundary retards horizontal fluid flow, resulting in the growth of vertical velocity gradients the extent of which define a velocity boundary layer (VBL). Owing to the exponential dependence of the viscosity of the syrup on temperature, the thickness of the velocity boundary layer depends strongly on the viscosity ratio λ . When $\lambda > 10$ the velocity boundary layer is confined to the lowest 10–15% of the thermal boundary layer, where the temperature is highest and, hence, the viscosity is lowest.

of the hot thermal-boundary-layer fluid is advected laterally at a velocity $u_t \sim U$. However, as $\lambda \rightarrow 1$ vertical velocity gradients extend increasingly from the boundary such that δ_v approaches a maximum height $H/2$ as drag increasingly retards horizontal flow. Therefore, most of the hot thermal-boundary-layer fluid is advected laterally at a velocity $u_t < U$.

Examination of Figs. 2 and 4 suggests that the influence of large-scale circulation on the thickness of the thermal boundary layer δ_t and the corresponding heat flux q may be analyzed in two viscosity ratio limits. When $\lambda \sim 10$ (Fig. 5a) the average horizontal velocity in the thermal

boundary layer $u_t \approx U$ and hence the base of the tank can be approximated as a free-slip boundary. In this limit, the global conservation of heat in the thermal boundary layer requires a balance between the vertical conduction of heat from the hot boundary and the lateral advection of heat by flow within the thermal boundary layer [38]:

$$\kappa \frac{\Delta T}{\delta_t^2} \sim U \frac{\Delta T}{L} \quad (5)$$

Using Eqs. 1–4 and noting that $L = 0.45AH$, this expression indicates a thermal boundary layer thickness that scales as:

$$\delta_t^f \sim \left(\frac{\kappa L}{U_v} \right)^{1/2} \sim H \left(\frac{0.45A}{\text{Pe}} \right)^{1/2} \quad (6)$$

which, in turn, implies a heat flux $q \sim K\Delta T/\delta_t$ of:

$$q^f = k_1 \frac{K\Delta T}{H} \left(\frac{1}{0.45} \frac{\text{Pe}}{A} \right)^{1/2} \quad (7)$$

Here, the constant of proportionality $k_1 \approx 0.74$, the superscript ‘f’ means ‘free slip’, and ‘ \sim ’ means ‘of the same order of magnitude as’.

In the alternative limit of $\lambda \sim 1$, $\delta_t \ll \delta_v$, the average horizontal velocity $u_t < U$, and u_t is a function of both U and λ , since the base of the tank is a ‘no-slip’ boundary. Following the qualitative argument of Morris [37] and Morris and Canright [38], in this case the flow may be divided into two superposed layers, with the thermal boundary layer forming the bottom layer and the majority of the velocity boundary layer forming a top layer with an approximate thickness $H/2$ (Fig. 4b). For this situation we again consider the global conservation of heat in the thermal boundary layer. From Eq. 6 we obtain a scale for average horizontal velocity:

$$u_t \sim \frac{0.45\kappa AH}{\delta_t^2} \quad (8)$$

With Eqs. 1–4 and the additional requirement that stress and velocity be continuous across the viscosity interface separating the two layers [$\mu_s(u_t/\delta_t) \sim \mu_l(2U/H)$], the boundary layer thickness is given by:

$$\delta_t^n \sim H \left(\frac{0.23A}{\lambda \text{Pe}} \right)^{1/3} \quad (9)$$

and the corresponding heat flux from the boundary is:

$$q^n = k_2 \frac{K\Delta T}{H} \left(\frac{2\lambda \text{Pe}}{0.45A} \right)^{1/3} \quad (10)$$

where the superscript ‘n’ means ‘no slip’ and the constant $k_2 \approx 1.24$. The 1/3 and 1/2 powers in Eqs. 7 and 10 are consistent with classical free-slip and no-slip scalings determined for steady flows [39,40]. Significantly, that we recover these classical results indicates that they may be extended to the case of the unsteady flow of a fluid with a temperature-dependent viscosity over a hot, rigid boundary. Eqs. 7 and 10 are also consistent with solutions obtained by Morris [37] for the steady flow of a fluid with a temperature-dependent viscosity past a hot, rigid sphere. Furthermore, Eq. 7 is consistent with the analysis by Morris and Canright [38] of the steady flow of a fluid with a temperature-dependent viscosity in a horizontal thermal boundary layer overlying a free-slip surface.

Predicted heat flux ratios along with dimensional heat fluxes are plotted as a function of λ also in Fig. 5. Comparison with the data indicates that ‘no-slip’ and ‘free-slip’ approximations are valid when λ is less than and greater than about 5, respectively (i.e. order 10). For $\lambda > 5$, horizontal flow reduces the thermal boundary layer thickness at position L such that $\delta_t < \delta_t^{\text{max}}$, resulting in a factor of 2–3 increase in the basal heat flux over that which would occur as a consequence of the formation and rise of plumes alone. That the heat flux ratio $q^p/q \rightarrow 1$ when $\lambda < 3$ –5 is consistent with an observed transition from a flow dominated by large-scale stirring to one governed by the formation and rise of plumes. As Pe is fixed in this experiment we interpret this result to indicate that significant drag reduces the horizontal flow velocity in the thermal boundary layer such that $\delta_t \rightarrow \delta_t^{\text{max}}$ and $q \rightarrow q^p$.

5. Applications to the Earth

In exploring the implications of this study to the Earth we make three assumptions: (1) large-scale motions driven by plate subduction stir the full depth of the mantle (e.g. [41]), resulting in

upwellings in the central Pacific and beneath Africa [42] and possibly into ridges; (2) deep mantle plumes ascend from the core–mantle boundary (CMB); and (3) the viscosity ratio in the hot thermal boundary layer at the base of the mantle $\lambda > 100$ [43–46]. Given these restrictions, applying our results requires a constraint on the velocity ratio V , which we address next. After establishing a plausible range for mantle V we investigate the implications for the dependence of MORB geochemistry on spreading rate as well as current estimates of the core heat flux. We conclude with a discussion of the limitations of our analysis and directions for future work.

5.1. Estimate of the mantle velocity ratio V

Although surface plate velocities on the Earth are well determined [47], the potentially complicated way in which mantle viscosity increases with depth makes it difficult to predict an average V explicitly [41,42,48]. Fluid mechanical studies and estimates of melting rates in plumes suggest that plume heads probably rise through the mantle at an average speed of a few centimeters per year [41,44], and so the main uncertainty is the magnitude of horizontal flow speeds in the lower mantle. One approach to this problem is to infer these velocities from lateral density variations identified with tomographic models of the mantle. For example, the results from new and previous models presented in a recent study by Forte and Mitrovica [42] constrain the maximum flow velocities in the lower mantle to be around 2 cm yr^{-1} . Taking this velocity as an upper bound for the whole lower mantle, an average horizontal velocity, and thus V , depends on plate speed. Therefore, V appropriate for the slow-spreading (1–3 cm/yr) Mid-Atlantic Ridge (MAR)–southwest Indian Ridge (SWIR) system is order 1. A suitable V for the fast-spreading (8–10 cm/yr) East Pacific (EPR), Southeast Indian (SEI), and Pacific-Antarctic (PAR) ridges is order 10.

Fig. 2 shows that, depending on V , mantle upwellings due to plate-driven flow can influence the trajectories of plumes. Moreover, the surface expression of plumes (i.e. hotspots) is expected to occur near divergent boundaries and close to or

within the superswells overlying the well-documented deep mantle upwellings (e.g. [42]) beneath Africa and the central Pacific. Consequently, an alternative constraint on V may be to infer this parameter from the distribution of hotspots. Indeed, this approach is supported by the modeling efforts of Steinberger and O’Connell [24,25] and Steinberger [26], who find that mantle stirring driven by modern surface plate motions causes plume conduits at the base of the mantle to be drawn towards (hot) upwelling regions beneath the Pacific and Africa, and causes hotspots to occur preferentially near ridges.

Whether mantle plumes form hotspots at or near divergent boundaries probably depends on if they can rise through the mantle before being drawn into or ‘captured by’ underlying mantle upwellings. Interestingly, in addition to being clustered in the central Pacific and Africa (Fig. 6a (cf. [49,50])), hotspots appear to be concentrated near slow-spreading ridges, a suggestion first made by Weinstein and Olson [51]. Fig. 6a shows, for example, that in addition to the clusters of five and seven hotspots in the central Pacific and Africa, roughly 18 hotspots occur within about 1000 km of the MAR–SWIR system, while only about four to five hotspots occur close to the EPR–PAR and SEI ridges combined. (The total MAR–SWIR is comparable in length to the EPR–PAR, SEI system.)

Although Fig. 6a is a popular compilation of hotspots, whether all of the indicated hotspots are related to deep mantle plumes remains a matter for debate (e.g. [52]; Courtillot, personal communications, 2001). The distinction between hotspots and hotspots related to deep mantle plumes is important for this discussion because our experiments are designed to understand the formation and subsequent rise of plumes from a hot thermal boundary layer at the base of the mantle. Following Clouard and Bonneville [52] and Courtillot (personal communications, 2001), in Fig. 6b we show the distribution of hotspots that have a documented relationship to flood basalts [50] and/or that reflect volcanism over time scales comparable to or greater than the time for a plume to rise through the full depth of the mantle (order 10–100 Myr). We take this compilation to

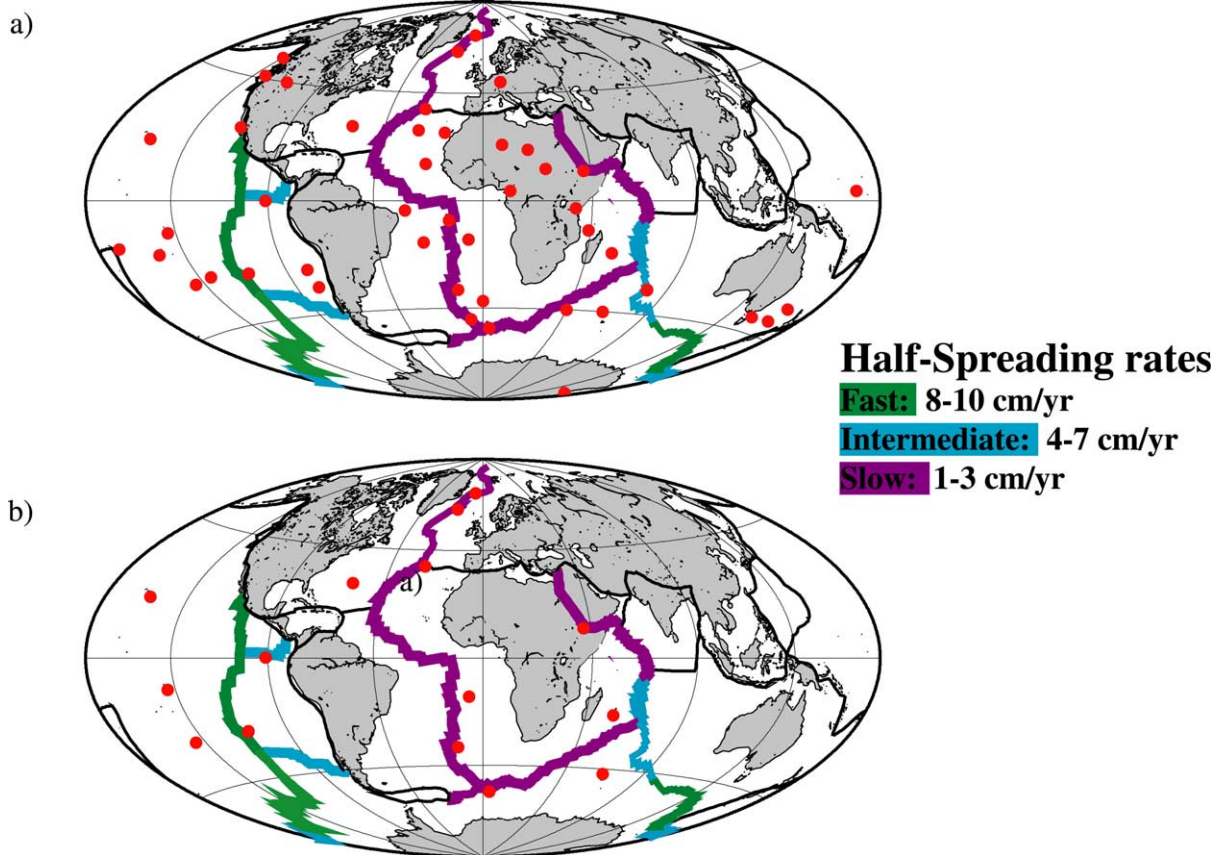


Fig. 6. Two maps showing the proposed global distributions of hotspots (red dots) along with the positions of spreading ridges on the Earth. Hotspots appear to be concentrated near slow-spreading ridges. In panel (a), which is a commonly cited compilation, whereas there are roughly 18 hotspots within about 1000 km of the slow-spreading mid-Atlantic ridge (MAR)–Southwest Indian ridge (SWIR) system, there are perhaps only four to five hotspots adjacent to the fast-spreading East Pacific Rise (EPR)–Pacific Antarctic ridge (PAR) system. In panel (b), we include only those hotspots that have been shown convincingly to be associated with mantle plumes ascending from the core–mantle boundary of the Earth (see text for discussion). In this compilation, whereas there are 10 hotspots along the MAR–SWIR system (11 if Galapagos, which is attributed to the Caribbean flood basalts, is included), there are only two (one if Galapagos is excluded) associated with the EPR–PAR system.

be a lower bound on the number of hotspots related to deep mantle plumes. In this data set, although African hotspots may be underrepresented, the correlation between hotspots and slow-spreading ridges is stronger: 10 hotspots are near the MAR–SWIR system and only two are proximal to the EPR–PAR system. We note that the Galapagos hotspot is generally associated with the Caribbean flood basalt. If so, then the ratio of hotspots associated with slow-spreading ridges to those associated with fast-spreading ridges increases to 11:1.

Our experimental results may offer new insight for interpreting the data in Fig. 6 that is consistent with the analysis of Steinberger [26]. Upwellings into the MAR are sufficiently strong to focus plumes toward the ridge, but insufficiently strong to capture them entirely; thus hotspots can form. From Fig. 2, we then *infer* V to be order 1. In contrast, mantle upwellings beneath fast ridges such as the EPR entrain most (but not all) ascending plumes resulting in few hotspots. Applying again the results in Fig. 2, we thus *infer* $1 < V < 10$, although the upper bound must de-

pend on the depth from which these flows originate. The clustering of hotspots in the central Pacific and possibly Africa suggests that plumes are drawn towards the strong upwellings beneath these areas [42] and, thus, that these upwellings imply a regime in which $V \geq 1$. These mantle velocity ratios are consistent with the analysis of KSD who argue that a similar range of velocity ratios $1 < V < 6$ (cf. Section 3) may explain why the topography and gravity of the MAR is spatially variable relative to the EPR. Finally, it is important to point out that, whether V is inferred using measured plate velocities and tomographic models or from the global distribution of hotspots, the results are consistent with one another.

5.2. Dependence of MORB chemistry on spreading rate

Assuming that mantle plume material is ‘enriched’ in light rare earth elements (LREEs) and radiogenic isotopes of Sr and Pb and depleted in radiogenic isotopes of Nd [53,54], our proposed hypothesis for the plume–ridge relationship carries a testable prediction for the dependence of MORB chemistry on spreading rate. Mantle flow due to fast ridges is expected to draw both plume and upper mantle components into a central upwelling, resulting in a uniformly enriched source region for the production of MORBs. Consequently, MORBs from a fast-spreading ridge should have relatively enriched LREE, Sr and Pb isotopic compositions, and depleted Nd isotopic compositions. Moreover, if the mixing of plume and mantle components is complete then MORBs from fast ridges should be chemically homogeneous along the length of a ridge. If mixing of the two components is incomplete, spatially random chemical excursions from the global mean may occur. Flow due to slow-spreading ridges, on the other hand, does not completely incorporate plumes into an underlying upwelling sheet, but instead produces nearby (or on-ridge) hotspots. As a result, both the source region for MORBs and the erupted products (i.e. ‘normal MORB’) are expected to be depleted in plume components.

That the variation of MORB chemistry with

spreading rate reflects differing extents of mixing of plume and upper mantle components has been inferred previously on geochemical grounds by Allegre et al. [55] and Langmuir et al. [6]. A number of studies of the LREE and isotopic geochemistry of basalts collected from the MAR and EPR support these predictions [6,56]. For example, Fig. 7a shows that MAR basalts have bimodal LREE compositions with $Ce/Sm \approx 2.7$ for normal MORB segments and Ce/Sm up to about 15 for narrow segments influenced by nearby hotspots [4–6]. Many studies of Atlantic hotspots have suggested that the flow of plume material from hotspots to the MAR has produced locally steep gradients as well as large absolute enrichments (relative to normal MORB) in the concentrations of LREE and certain radiogenic isotopes in samples of MORB [4–6,57–64].

In contrast, the LREE geochemistry of EPR basalts is fairly homogeneous and enriched in plume components relative to normal MORB with $Ce/Sm = 3.45 \pm 1.21$. Geochemical excursions do occur along the EPR but appear to be uncorrelated topographically or geochemically with nearby hotspots and are usually taken to be random [6,65]. Indeed, these anomalies may reflect variability in the local extent of mixing between plume and upper mantle components in the MORB source region. From the data presented in Fig. 7b,c, similar arguments can be made to explain the variability in $^{206}Pb/^{204}Pb$ and $^{143}Nd/^{144}Nd$ values with latitude.

5.3. Plume capture and the difficulty with estimating a core heat flux using hotspots

Estimates of the core heat flux based on the lithospheric thermal signatures of hotspots suggest that mantle plumes carry about 10% ($\sim 0.01 \text{ W m}^{-2}$) of the global mantle heat flux [66,67], which is sometimes taken to represent the core heat flux (e.g. [68–70]). Our experimental results and proposed hypothesis for plume–ridge interactions have two additional implications for estimating the magnitude of core cooling. First, depending on the aspect ratio and velocity of motions at the base of the mantle, $\delta_t < \delta_t^{\max}$ possibly over significant fractions of the surface of the

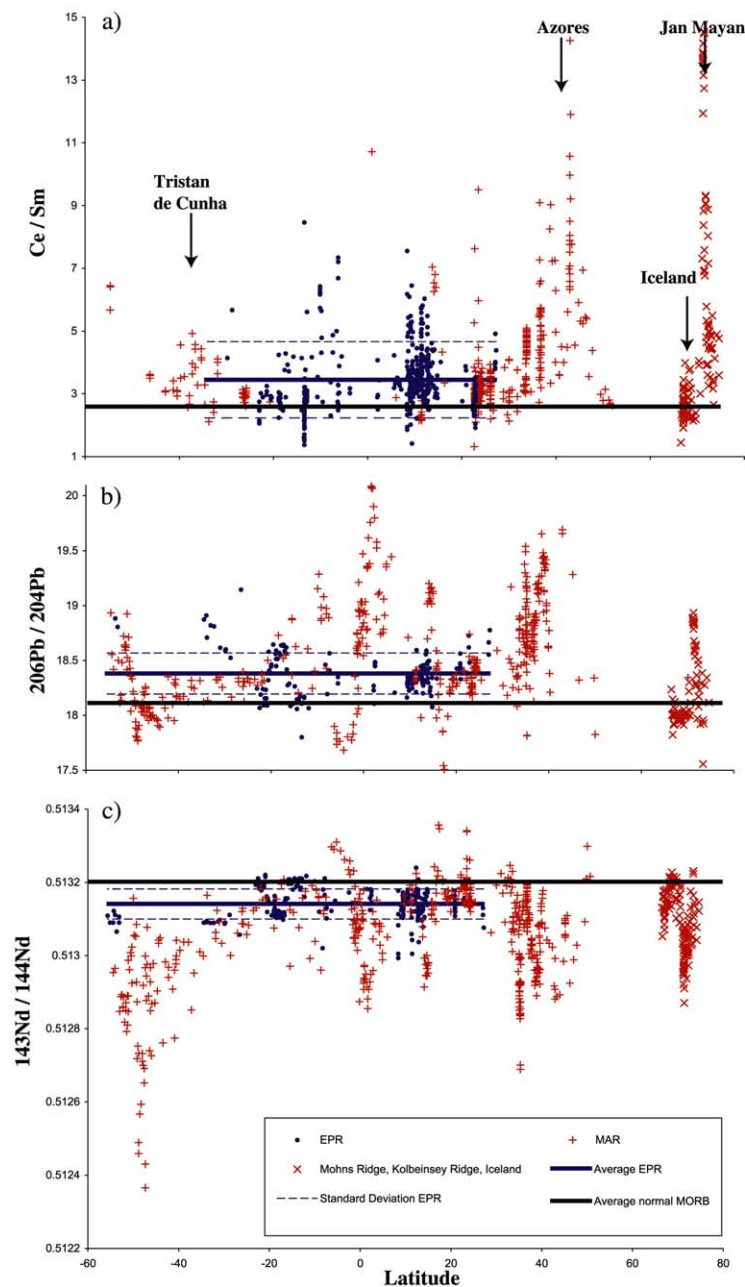


Fig. 7. Plots (a–c) of Ce/Sm, $^{206}\text{Pb}/^{204}\text{Pb}$, and $^{143}\text{Nd}/^{144}\text{Nd}$ ratios, which are from whole rock and glass analyses of MORBs collected over comparable lengths of the MAR (red) and EPR (blue), showing a variation of MORB geochemistry with spreading rate. Also indicated are the global mean values for these ratios with their standard deviations for EPR, along with approximate average normal MORB compositions obtained from segments of the MAR that are uninfluenced by hotspots. Data from EPR MORB show greater homogeneity and greater enrichment in incompatible (plume) components relative to ‘normal’ MAR MORB. Data from MAR MORB are highly variable with steep gradients over 5–10 degrees of latitude occurring in segments influenced by hotspots (see text for discussion). The data are from [4–6] and the RIDGE PETDB database at the Lamont Doherty Earth Observatory (<http://petdb.ldeo.columbia.edu/petdb/>).

core–mantle boundary, resulting in a variable and potentially larger average core heat flux than that due to the formation and rise of plumes alone. Second, even if $\delta_t = \delta_t^{\max}$ and plumes form everywhere along the core–mantle boundary, if $1 \leq V < 10$ a potentially significant fraction of these upwellings may be captured by large-scale mantle flow and carried into ridges. An important implication of this result is that the number of hotspots observed at the Earth's surface may represent only a fraction of the number of plume instabilities forming at the base of the mantle. Labrosse [71] has recently raised a similar concern over the sampling of mantle plumes by arguing that only a modest proportion of these upwellings may have sufficient thermal buoyancy to cross the mantle and form a hotspot. Both our and Labrosse's arguments suggest that estimates of the core heat flux based on a total core heat flow inferred from hotspots may imply only a weak lower bound on the actual core heat flux.

5.4. Questions and future directions: Towards a viable hypothesis

Our results raise some difficult questions that need to be addressed in future studies. In order for the proposed variable mixing of plume material into upwellings beneath ridges to be a viable hypothesis *both* variations in MORB chemistry and variations in the ratio of core to mantle heat flux carried up into ridges with spreading rate must be self-consistent. If these two indicators can be shown to be consistent with one another our results strengthen the suggestion that the distribution of hotspots is determined by the positions of ridges and their attendant spreading rates, which is also suggested by the results of Steinberg and O'Connell [24–26]. Consequently, potentially the most important issue to resolve in the future is the expression of core heat flux at ridges and in the broad upwellings beneath the central Pacific and Africa; in particular, whether the buoyancy of hot rising plume material beneath fast-spreading centers would cause large (and currently unobserved) dynamic topography and geoid anomalies over, for example, the EPR.

Richards and Hager [72] argue that the lack of

any consistent long-wavelength geoid signal over mid-ocean ridges is inconsistent with active upwellings feeding ridges. Davies [66,73] and Davies and Richards [41] argue further that large topographic and geoid anomalies over active upwelling sheets left behind by migrating ridges would be an obvious (and also unobserved) consequence of a large component of heat transfer associated with such upwellings. However, Davies' calculations can allow for as much as a factor of three increase in the amount of heat carried into ridges. Thus, further investigation of the oceanic geoid and bathymetry is warranted and might offer an additional constraint on the degree to which large-scale mantle flow governs the heat flux from the core.

There are, however, two significant complications for any study of dynamic topography that must be addressed carefully in future numerical studies. First, both dynamic topography and the geoid are sensitive to the viscosity structure of the mantle. In particular, buoyant plume material may spread laterally into a low-viscosity asthenosphere [73], resulting in a relatively suppressed (lower amplitude, longer wavelength) topographic signal at the surface. Indeed, results from the recent MELT experiment have suggested that the mantle underlying the EPR is compositionally and rheologically complex, apparently characterized by an asymmetrical melt distribution across the ridge axis [74–77]. Thus, the influence of additional buoyancy due to plumes on the topography and geoid at the EPR is potentially very complicated. Second, the expression of core heat flux at ridges is sensitive to the viscosity ratio λ . In addition to overly simplified models for the viscosity stratification in the mantle, the models of Davies [66,73], for example, employ smaller viscosity ratios ($\lambda=5$ and 30) than suggested for mantle plumes in the Earth ($\lambda > 100$) [43–46]. The cross-sectional width of a buoyant upwelling sheet and, hence, the associated geoid and topographic signatures, decreases with increasing λ . Data from our laboratory experiments cannot accurately predict geoid and topographic signals that would be associated with analogous upwelling flows in the Earth. Therefore, further numerical investigations of the influences of large viscosity contrasts on

these observable features, in which up-to-date models of the radial variations of mantle viscosity are employed, is warranted. Furthermore, the ‘active’ upwelling sheets that result in some of our models will clearly follow ridge migration. Thus, an additional important issue is the identification and characterization of ridge seismic velocity anomalies associated with such low-viscosity upwellings.

In order to better understand the apparent systematic variation of MORB geochemistry with spreading rate additional sampling is needed along the EPR and MAR as well as along the other ridge systems around the world. Also, as speculated by Kincaid et al. [23], the results shown in Figs. 4 and 5 may be applied to explain the well-known observation that fast ridges (EPR) tend to produce smoother topography than slow ridges (MAR), but we cannot demonstrate a quantitative connection at this time.

Finally, the proposed entrainment of plumes into deep mantle upwellings beneath the central Pacific and Africa raises the possibility that buoyant plume material augments the dynamic topography associated with the structure of mantle return flow driven by plate subduction [78]. Whether this additional buoyancy can plausibly explain the anomalously large topographic ‘super-swells’ currently observed in the central Pacific and Africa [79], as well as the large rate of volcanism associated with the concentration of hot-spots [79], remains an exciting direction for future study.

Acknowledgements

We thank Geoff Davies, Garrett Ito, Peter Olson and Paul Tackley for detailed reviews that vastly improved this manuscript. We also thank Stephen Zatman, Michael Manga, Ross Griffiths, Vincent Courtillot and Francis Albarede for useful discussions and comments. John Donovan and Dave Smith assisted in the design and construction of the experimental apparatus. We also thank the Archers-Daniels-Midland Company for faithfully delivering immense quantities of corn syrup at cost. This work was supported by a National

Science Foundation grant to M.A.R., and the Miller Institute for Basic Research in Science. [SK]

References

- [1] J.T. Wilson, A possible origin of the Hawaiian Islands, *Can. J. Phys.* 41 (1963) 863–870.
- [2] W.J. Morgan, Convection plumes in the lower mantle, *Nature* 230 (1971) 42–43.
- [3] P.J. Tackley, Mantle convection and plate tectonics: Toward an integrated physical and chemical theory, *Science* 288 (2000) 2002–2007.
- [4] J.-G. Schilling, M. Zajac, R. Evans, T. Johnston, W. White, J.D. Devine, R. Kingsley, Petrologic and geochemical variations along the Mid-Atlantic Ridge from 29-degrees-N to 73-degrees-N, *Am. J. Sci.* 28 (1983) 510–586.
- [5] J.-G. Schilling, Geochemical and isotopic variation along the Mid-atlantic ridge axis from 79° N to 0° N, in: P.R. Vogt, B.E. Tucholke (Eds.), *The Geology of North America*, Vol. M, The Western North Atlantic Region, *Geol. Soc. Am.*, 1986, pp. 137–156.
- [6] C.H. Langmuir, E.M. Klein, T. Plank, Petrological systematics of mid-ocean ridge basalts: Constraints on melt generation beneath ocean ridges, in: J. Phipps Morgan, D.K. Blackman, J.M. Sinton (Eds.), *Mantle Flow and Melt Generation at Mid-Ocean Ridges*, *AGU Geophys. Monograph* 71 (1992) 183–280.
- [7] C. Small, Observations of ridge-hotspot interactions in the Southern-Ocean, *J. Geophys. Res.* 100 (1995) 17931–17946.
- [8] D. Peate, C.J. Hawkesworth, P.W. van Calsteren, R.N. Taylor, B.J. Murton, ^{238}U - ^{230}Th constraints on mantle upwelling and plume-ridge interaction along Reykjanes Ridge, *Earth Planet. Sci. Lett.* 187 (2001) 259–272.
- [9] M. Abelson, A. Agnon, Hotspot activity and plume pulses recorded by geometry of spreading axes, *Earth Planet. Sci. Lett.* 189 (2001) 31–47.
- [10] G. Ito, J. Lin, D. Graham, Observational and theoretical studies of the dynamics of mantle plume-mid-ocean ridge interaction, *Rev. Geophys.* (in press).
- [11] N. Ribe, U.R. Christensen, J. Theissing, The dynamics of plume-ridge interaction, 1: Ridge-centered plumes, *Earth Planet. Sci. Lett.* 134 (1995) 155–168.
- [12] N. Ribe, The dynamics of plume-ridge interaction 2. Off-ridge plumes, *J. Geophys. Res.* 101 (1996) 16195–16204.
- [13] N. Ribe, W.L. Delattre, The dynamics of plume-ridge interaction, 3: The effects of ridge migration, *Geophys. J. Int.* 133 (1998) 511–518.
- [14] G. Ito, J. Lin, Oceanic spreading center-hotspot interactions Constraints from along-isochron bathymetric and gravity anomalies, *Geology* 23 (1995) 657–660.
- [15] E.M. Parmentier, J.P. Morgan, Spreading rate dependence of 3-dimensional structure in oceanic spreading centers, *Nature* 348 (1990) 325–328.

- [16] J.P. Morgan, E.M. Parmentier, J. Lin, Mechanisms for the origin of midocean ridge axial topography - implications for the thermal and mechanical structure of accreting plate boundaries, *J. Geophys. Res.* 92 (1987) 12823–12836.
- [17] M. Rabinowicz, S. Rouzo, S. Sempere, J.C. Rosemberg, 3-dimensional mantle flow beneath midocean ridges, *J. Geophys. Res.* 98 (1993) 7851–7869.
- [18] M.A. Feighner, M.A. Richards, The fluid-dynamics of plume-ridge and plume-plate interactions: an experimental investigation, *Earth Planet. Sci. Lett.* 129 (1995) 171–182.
- [19] C. Kincaid, G. Ito, C. Gable, Laboratory investigation of the interaction of off-axis mantle plumes and spreading centers, *Nature* 376 (1995) 758–761.
- [20] M.A. Feighner, L.H. Kellogg, B.J. Travis, Numerical modeling of chemically buoyant mantle plumes at spreading ridges, *Geophys. Res. Lett.* 22 (1995) 715–718.
- [21] G. Ito, J. Lin, C.W. Gable, Dynamics of mantle flow and melting at a ridge-centered hotspot: Iceland and the Mid-Atlantic Ridge, *Earth Planet. Sci. Lett.* 144 (1996) 53–74.
- [22] M. Albers, U.R. Christensen, Channeling of plume flow beneath mid-ocean ridges, *Earth Planet. Sci. Lett.* 187 (2001) 207–220.
- [23] C. Kincaid, D.W. Sparks, R. Detrick, The relative importance of plate-driven and buoyancy-driven flow at mid-ocean ridges, *J. Geophys. Res.* 101 (1996) 16177–16193.
- [24] B. Steinberger, R.J. O’Connell, Advection of plumes in mantle flow: implications for hotspot motion, mantle viscosity, and plume distribution, *Geophys. J. Int.* 132 (1998) 412–434.
- [25] B. Steinberger, R.J. O’Connell, Effects of mantle flow on hotspot motion, in: M.A. Richards et al. (Eds.), *The History and Dynamics of Global Plate Motions*, AGU Monograph 121 (2000) 377–398.
- [26] B. Steinberger, Plumes in a convecting mantle: Models and observations for individual hotspots, *J. Geophys. Res.* 105 (2000) 11127–11152.
- [27] C. Lithgow-Bertelloni, M.A. Richards, R.W. Griffiths, C. Conrad, Plume generation in natural thermal convection at high Rayleigh and Prandtl numbers, *J. Fluid Mech.* 434 (2001) 1–21.
- [28] J.S. Turner, *Buoyancy Effects in Fluids*, Cambridge Univ. Press, Cambridge, 1973, 368 pp.
- [29] A. Davaille, C. Jaupart, Transient high-Rayleigh-number thermal-convection with large viscosity variations, *J. Fluid Mech.* 253 (1993) 141–166.
- [30] A.M. Jellinek, R.C. Kerr, R.W. Griffiths, Mixing and compositional stratification produced by natural convection 1. Experiments and their application to Earth’s core and mantle, *J. Geophys. Res.* 104 (1999) 7183–7202.
- [31] D. Weeraratne, M. Manga, Transitions in the style of mantle convection at high Rayleigh numbers, *Earth Planet. Sci. Lett.* 160 (1998) 563–568.
- [32] M. Manga, D. Weeraratne, Experimental study of non-Boussinesq Rayleigh-Bernard convection at high Rayleigh and Prandtl numbers, *Phys. Fluids* 11 (1999) 2969–2977.
- [33] F. Selig, A theoretical prediction of salt dome patterns, *Geophysics* 30 (1965) 633–643.
- [34] J.R. Lister, R.C. Kerr, The effect of geometry on the gravitational-instability of a buoyant region of viscous fluid, *J. Fluid Mech.* 202 (1989) 577–594.
- [35] R. Krishnamurti, On transition to turbulent convection, 1. Transition from 2-dimensional to 3-dimensional flow, *J. Fluid Mech.* 42 (1970) 295–307.
- [36] R. Krishnamurti, On transition to turbulent convection, 2. Transition to time-dependent flow, *J. Fluid Mech.* 42 (1970) 308–320.
- [37] S. Morris, The effect of a strongly temperature-dependent viscosity on slow flow past a hot sphere, *J. Fluid Mech.* 124 (1982) 1–26.
- [38] S. Morris, D. Canright, A boundary-layer analysis of Bernard convection in a fluid of strongly temperature-dependent viscosity, *Phys. Earth Planet. Inter.* 36 (1984) 355–373.
- [39] A. Acrivos, J.D. Goddard, Asymptotic expansions for laminar convection heat and mass transfer, *J. Fluid Mech.* 23 (1965) 273–291.
- [40] L.G. Leal, *Laminar Flow and Convective Transport Processes*, Butterworth-Heinemann, Boston, 1992, 740 pp.
- [41] G.F. Davies, M.A. Richards, Mantle convection, *J. Geol.* 100 (1992) 151–206.
- [42] A.M. Forte, J.X. Mitrovica, Deep mantle high viscosity flow and thermochemical structure inferred from seismic and geodynamic data, *Nature* 402 (2001) 1881–1884.
- [43] M.A. Richards, R.A. Duncan, V.E. Courtillot, Flood basalts and hot-spot tracks: plume heads and tails, *Science* 246 (1989) 103–107.
- [44] R.W. Griffiths, I.H. Campbell, *Earth Planet. Sci. Lett.* 99 (1990) 66–78.
- [45] J.-G. Schilling, Fluxes and excess temperatures of mantle plumes inferred from their interaction with migrating mid-ocean ridges, *Nature* 352 (1991) 397–403.
- [46] D.E. Loper, F.D. Stacey, The dynamical and thermal structure of deep mantle plumes, *Phys. Earth Planet. Inter.* 33 (1983) 304–317.
- [47] C. DeMets, R.G. Gordon, D.F. Argus, S. Stein, Current plate motions, *Geophys. J. Int.* 101 (1990) 425–478.
- [48] K. Lambeck, P. Johnston, The viscosity of the mantle: evidence from analyses of glacial-rebound phenomena, in: I. Jackson (Ed.), *The Earth’s Mantle: Composition, Structure, and Evolution*, Cambridge Univ. Press, New York, 1998, pp. 461–503.
- [49] M.A. Richards, B.H. Hager, N.H. Sleep, Dynamically supported geoid highs over hotspots: observation and theory, *J. Geophys. Res.* 93 (1988) 7690–7708.
- [50] R.A. Duncan, M.A. Richards, Hotspots, mantle plumes, flood basalts, and true polar wander, *Rev. Geophys.* 29 (1991) 31–50.
- [51] S.A. Weinstein, P.L. Olson, The proximity of hotspots to convergent and divergent plate, *Geophys. Res. Lett.* 16 (1989) 433–436.
- [52] V. Clouard, A. Bonneville, How many Pacific hotspots are fed by deep-mantle plumes?, *Geology* 29 (2001) 695–698.

- [53] J.-G. Schilling, Iceland mantle plume geochemical study of Reykjanes ridge, *Nature* 242 (1973) 565–571.
- [54] A.W. Hoffmann, Mantle chemistry the message from oceanic volcanism, *Nature* 385 (1997) 219–229.
- [55] C.J. Allegre, B. Hamelin, B. Dupre, Statistical-analysis of isotopic-ratios in MORB: The mantle blob cluster model and the convective regime of the mantle, *Earth Planet. Sci. Lett.* 71 (1984) 71–84.
- [56] M.B. Holness, F.M. Richter, Possible effects of spreading rate on MORB isotopic and rare-earth composition arising from melting of a heterogeneous source, *J. Geol.* 97 (1989) 247–260.
- [57] P.R. Vogt, The Iceland phenomenon; imprints of a hot spot on the ocean crust, and implications for flow below the plates, in: L. Kristjanson (Ed.), *Geodynamics of Iceland and the North Atlantic Area*, Proceedings of the NATO Advanced Study Institute, University of Iceland, Reykjavik, Iceland, July 1–7, 1974, Kluwer Academic, 1974, pp. 105–126.
- [58] W.J. Morgan, Rodriguez, Darwin, Amsterdam... 2nd type of hotspot island, *J. Geophys. Res.* 83 (1978) 5355–5360.
- [59] G.E. Vink, A hotspot model for Iceland and the Voring plateau, *J. Geophys. Res.* 89 (1984) 9949–9959.
- [60] J.-G. Schilling, Upper mantle heterogeneities and dynamics, *Nature* 314 (1985) 62–67.
- [61] J.-G. Schilling, G. Thompson, R. Kingsley, S. Humphris, Hotspot - migrating ridge interaction in the South-Atlantic, *Nature* 313 (1985) 187–191.
- [62] B.B. Hanan, R.H. Kingsley, J.-G. Schilling, Pb isotope evidence in the South-Atlantic for migrating ridge hotspot interactions, *Nature* 322 (1986) 137–144.
- [63] C. Small, Observations of ridge-hotspot interactions in the Southern-Ocean, *J. Geophys. Res.* 100 (1995) 17931–17946.
- [64] J. Phipps Morgan, W.J. Morgan, Y.S. Zhang, W.H.F. Smith, Observational hints for a plume-fed, suboceanic asthenosphere and its role in mantle convection, *J. Geophys. Res.* 100 (1995) 12753–12767.
- [65] J.J. Mahoney, J.M. Sinton, M.D. Kurz, J.D. Macdougall, K.J. Spencer, G.W. Lugmair, Isotope and trace-element characteristics of a super-fast spreading ridge - East Pacific Rise, 13-23-degrees-S, *Earth Planet. Sci. Lett.* 121 (1994) 173–193.
- [66] G.F. Davies, Ocean bathymetry and mantle convection, I. Large-scale flow and hotspots, *J. Geophys. Res.* 93 (1988) 10467–10480.
- [67] N.H. Sleep, Hotspots and mantle plumes: Some phenomenology, *J. Geophys. Res.* 95 (1990) 6715–6736.
- [68] F.D. Stacey, D.E. Loper, Thermal histories of the core and mantle, *Phys. Earth Planet. Inter.* 36 (1984) 99–115.
- [69] U. Christensen, Instability of a hot boundary-layer and initiation of thermo-chemical plumes, *Anal. Geophys.* 2 (1984) 311–320.
- [70] B.A. Buffett, H.E. Huppert, J.R. Lister, A.W. Woods, On the thermal evolution of the Earth's core, *J. Geophys. Res.* 101 (1996) 7989–8006.
- [71] S. Labrosse, Hotspots, mantle plumes and core heat loss, *Earth Planet. Sci. Lett.* 61 (2002) 1–10.
- [72] M.A. Richards, B.H. Hager, The Earth's geoid and the large-scale structure of mantle convection, in: S.K. Runcom (Ed.), *The Physics of the Planets*, Wiley, 1988, pp. 247–272.
- [73] G.F. Davies, Effect of a low viscosity layer on long-wavelength topography, upper mantle case, *Geophys. Res. Lett.* 16 (1989) 625–628.
- [74] J.P. Canales, R.S. Detrick, S. Bazin, A.J. Harding, J.A. Orcutt, Off-axis crustal thickness across and along the East Pacific Rise within the MELT area, *Science* 280 (1998) 1218–1221.
- [75] D.R. Toomey, W.S.D. Wilcock, S.C. Solomon, W.C. Hammond, J.A. Orcutt, Mantle seismic structure beneath the MELT region of the East Pacific Rise from P and S wave tomography, *Science* 280 (1998) 1224–1227.
- [76] R.A. Dunn, D.R. Toomey, R.S. Detrick, W.S.D. Wilcock, Continuous mantle melt supply beneath an overlapping spreading center on the East Pacific Rise, *Science* 291 (2001) 1955–1958.
- [77] D.R. Toomey, W.S.D. Wilcock, J.A. Conder, D.W. Forsyth, J.D. Blundy, E.M. Parmentier, W.C. Hammond, Asymmetric mantle dynamics in the MELT region of the East Pacific Rise, *Earth Planet. Sci. Lett.* 200 (2002) 287–295.
- [78] M.A. Richards, D.C. Engebretson, Large-scale mantle convection and the history of subduction, *Nature* 355 (1992) 437–440.
- [79] M. McNutt, Superswells, *Rev. Geophys.* 36 (1998) 211–244.